OXSR1 inhibits inflammasome activation by limiting potassium efflux during mycobacterial infection.

Elinor Hortle[1,2]*, Lam Vi Tran[1], Angela RM Fontaine[3], Natalia Pinello[4,5], Justin J-L Wong[4,5], Warwick J Britton[1,6], Stefan H Oehlers[1,2] *

[1] Tuberculosis Research Program Centenary Institute, The University of Sydney, Camperdown, NSW 2050, Australia

[2] The University of Sydney, Discipline of Infectious Diseases & Immunology and Marie Bashir Institute, Camperdown, NSW 2050, Australia

[3] Centenary Imaging and Sydney Cytometry at the Centenary Institute, The University of Sydney, Camperdown, NSW 2050, Australia

[4] Epigenetics and RNA Biology Program Centenary Institute, The University of Sydney, Camperdown, NSW 2050, Australia

[5] The University of Sydney, Faculty of Medicine and Health, Camperdown, NSW 2050, Australia

[6] Department of Clinical Immunology, Royal Prince Alfred Hospital, Camperdown, NSW 2050, Australia

* Co-corresponding author emails: stefan.oehlers@sydney.edu.au and e.hortle@centenary.org.au

Summary

Pathogenic mycobacteria inhibit inflammasome activation as part of their pathogenesis. While it is known that potassium efflux is a trigger for inflammasome activation, the

interaction between mycobacterial infection, potassium efflux and inflammasome activation has not been investigated. Here we use *Mycobacterium marinum* infection of zebrafish embryos and *Mycobacterium tuberculosis* of human THP-1 cells to demonstrate that pathogenic mycobacteria upregulate the host WNK signalling pathway kinases SPAK and OXSR1 which control intracellular potassium balance. We show that genetic depletion or inhibition of OXSR1 decreases bacterial burden and intracellular potassium levels. The protective effects of OXSR1 depletion are mediated by NLRP3 inflammasome activation and are dependent on caspase-mediated release of IL-1β and the downstream activation of protective TNF-α. The elucidation of this druggable pathway to potentiate inflammasome activation provides a new avenue for the development of host-directed therapies against intracellular infections.

Introduction

Inflammasomes are large cytosolic multi-protein complexes that are critical for the immune response to infection. They facilitate the production of bioactive IL-1β[1], which directs pathogen killing through upregulation of TNF-α[2] and orchestrates systemic immune control through paracrine signalling. Inflammasomes typically consist of a sensor protein, which detects specific stimuli within the cytosol, and an adaptor protein which facilitates the oligomerization of the sensor with pro-caspase-1 [3,4]. Inflammasome assembly triggers activation of caspase-1, which then cleaves pro-IL-1β and pro-IL-18 into their active forms. Caspase-1 also cleaves Gasdermin D, the N-terminal fragment of which forms pores in the cell membrane, allowing secretion of active IL-1β and IL-18, and triggering cell death via pyroptosis [4]. These events contribute to host defence by both rapidly inducing the inflammatory response and limiting replication of intracellular pathogens.

To escape this immune control, many successful intracellular pathogens have evolved methods to limit inflammasome activation [3]. Influenza A, *Pseudomonas aeruginosa*, Baculovirus, Vaccinia virus, *Streptococcus pneumoniae*, Myxoma virus and *Yersinia pseudotuberculosis* have all been shown to limit IL-1β production by inhibiting caspase-1 activation[3]. In the case of pathogenic mycobacteria, their interactions with inflammasome activation are more complex. One study has shown that *Mycobacterium tuberculosis* actively inhibits inflammasome activation via a zinc metalloprotease[5], and that clinical isolates associated with severe disease evade NLRP3 activation [6]. Others have shown that *M. tuberculosis* induces both NLRP3 inflammasome and caspase-1 activation [7-9]. Further studies suggest that *M. tuberculosis* actively inhibits activation of the AIM2 inflammasome and dampens activation of the NLRP3 inflammasome by upregulation of NOS and IFN-β[1,9-12].

The NLRP3 inflammasome, one of the best studied inflammasomes, can be triggered by numerous stimuli, including ATP, heme, pathogen-associated RNA, and a variety of bacterial components[13-17]. Because these triggers are so diverse, it has been suspected that these activation stimuli are not detected by NLRP3 directly, but rather NLRP3 activation is the result of converging cellular signals. There is evidence that mitochondrial dysfunction, reactive oxygen species, and lysosomal damage contribute to NLRP3 activation (as reviewed elsewhere [18,19]). A common event that occurs downstream of almost every NLRP3 stimulus is potassium (K^+) efflux. Studies have shown that K^+ ionophores stimulate NLRP3[20], that high extracellular K^+ can inhibit NLRP3 activation[21,22], and that K^+ efflux alone is sufficient to activate the NLRP3 inflammasome[23]. Although the mechanism linking K^+ efflux to activation of NLRP3 is not well defined, evidence suggests that K^+ efflux occurs upstream of NLRP3

activation and may induce a conformational change in NLRP3 that favours oligemerization[23,24]. This raises the possibility that K^+ efflux pathways could be targeted to therapeutically activate, or potentiate the activation of, NLRP3 to control intracellular pathogens.

One of the master regulators of cellular K^+ flux is the With-No-Lysine (WNK) kinase signalling pathway. In response to cellular stress or osmotic changes, WNK kinase activates the SPAK and OXSR1 kinases. SPAK and OXSR1 inhibit the KCC channels, which pump K^+ out of the cell, and activate the NKCC channels, which pump K^+ into the cell[25]. It has previously been shown that blocking the interaction of SPAK/OXSR1 and KCC1 leads to net K^+ efflux from the cell[26]. We have further shown that constitutively active KCC1 alters the inflammatory response to malaria infection in mice, and that this effect is associated with dramatically increased survival[27]. Here we sought to investigate whether the SPAK/OXSR1 pathway is involved in the host response to mycobacterial infection, and if this pathway could be manipulated as a host-directed therapy against infection.

Results

Infection-induced activation of *oxsr1a* aids the growth of pathogenic mycobacteria.

To determine if SPAK and OXSR1 are involved in immunity, we infected zebrafish embryos with *Mycobacterium marinum* and analysed gene expression at 3 days post infection (dpi). Both *stk39* and *oxsr1a* (the zebrafish orthologs of *SPAK* and *OXSR1* respectively) were significantly upregulated at 3 dpi compared to uninfected embryos (Figure 1A). This result is consistent with previous data showing *oxsr1a* is upregulated in *M. marinum*-infected macrophages[28].

To determine if the upregulation of *stk39* and *oxsr1a* results in increased bacterial growth, we depleted each kinase individually by CRISPR-Cas9 knockdown and infected the embryos with fluorescent *M. marinum* (Extended Data 1). *M. marinum* burden was significantly reduced in *oxsr1a*, but not *stk39*, knockdown embryos (Figures 1B and 1C). To confirm these results, we created a stable *oxsr1a* knockout allele $oxsr1a^{syd5}$(Extended Data 2). Homozygous, but not heterozygous, $oxsr1a^{syd5}$ embryos showed reduced bacterial burden (Figure 1D).

The immunomodulatory role of OXSR1 is conserved in human cells.

To determine whether the immunomodulatory role of OXSR1 is conserved across species, we first differentiated human THP-1 cells with PMA and infected with *M. tuberculosis.* At 3 dpi OXSR1 protein expression was significantly upregulated in infected cells compared to uninfected cells (Figure 2A and Extended Data 3), mirroring the increased *oxsr1a* expression observed in infected zebrafish embryos. To determine whether this upregulation would affect bacterial burden, we generated an *OXSR1* knockdown human THP-1 cell line (Figures 2B and Extended Data 3).

We first differentiated these THP-1 knockdown cells with PMA and infected with *M. marinum* to determine if mycobacterial infection would induce changes in intracellular K^+ concentration. While we saw a small, statistically insignificant, increase in intracellular K^+ concentration in *M. marinum*-infected control siRNA-expressing cells, *M. marinum*-infected *OXSR1* knockdown cells had significantly reduced K^+ concentration compared to uninfected *OXSR1* knockdown cells (Figure 2C).

We next infected our *OXSR1* knockdown THP-1 cells with *M. marinum* and *M. tuberculosis* H37Rv and quantified bacterial growth by CFU recovery. At 1 dpi, knockdown THP-1 cells had reduced intracellular *M. marinum* load compared to control THP-1 cells (Figure 2D). At 3 dpi, knockdown THP-1 cells had reduced intracellular *M. tuberculosis* load compared to WT THP-1 cells (Figure 2E).

Together these results indicate that OXSR1 controls cellular potassium flux during mycobacterial infection and that the immunomodulatory role of OXSR1 is conserved between zebrafish and humans.

Small molecule inhibition of SPAK/OXSR1 is host protective

Because SPAK/OXSR1-modulated K^+ channels also shuttle Cl^-, Na^{2+} and Ca^{2+}, this pathway has been studied for its role in hypertension. The small molecule, Compound B (CB), reduces hypertension in animal models by inhibiting WNK phosphorylation of SPAK/OXSR1[29], preventing SPAK/OXSR1 activation[30]. We first determined that 1.8 µM was the maximum dose of CB that could be tolerated by zebrafish larvae for 5 days for infection (Table 4). This concentration of CB did not affect the growth of *M. marinum* in axenic culture (Figure 3A).

Immersion of *M. marinum*-infected zebrafish embryos in 1.8 µM CB immediately after infection replicated the effect of *oxsr1a* knockdown by decreasing bacterial burden (Figure 3B). Treatment of infected THP-1 cells with CB also phenocopied the effect of *OXSR1* knockdown, with reduced *M. marinum* burden at 1 dpi (Figure 3C) and reduced *M. tuberculosis* H37Rv burden at 3 dpi compared to DMSO treatment (Figure 3D).

The *M. marinum* ESX1 secretion system is required for infection-induced upregulation of host *oxsr1a*.

We next examined the role of mycobacterial virulence in driving infection-induced expression of *oxsr1a* and sensitivity to Oxsr1a depletion or inhibition by infecting zebrafish embryos with ΔESX1 *M. marinum*, which cannot escape the macrophage phagocytic vacuole and fails to activate the inflammasome[31]. In contrast to infections with WT *M. marinum*, we did not observe an upregulation of either kinase when zebrafish embryos were infected with ΔESX1 *M. marinum* (Figure 4A). The burdens of zebrafish embryos infected with ΔESX1 *M. marinum* were unsensitive *oxsr1a* knockdown (Figure 4B) or treatment with CB (Figure 4C) suggesting a potential role for inflammasome activation in the protective effects of Oxsr1a depletion or inhibition.

Infection-induced OXSR1 suppresses inflammasome activity to aid mycobacterial infection.

To determine if the reduced bacterial burden in *oxsr1a* knockdown was mediated by increased inflammasome activation, we used CRISPR to knockdown *si:zfos-364h11.1*, a zebrafish protein with orthology to mouse and rat NLRP3, hereafter referred to as *nlrp3*, and the *il1b* gene which encodes IL-1β (Extended Data 1). Knockdown of *nlrp3* alone did not affect the *M. marinum* burden but ameliorated the protective effect of *oxsr1a* knockdown against *M. marinum* infection (Figures 5A and 5B). The same effect was observed in zebrafish embryos subjected to *il1b* knockdown in combination with *oxsr1a* knockdown during *M. marinum* infection (Figure 5C).

In THP-1 cells infected with *M. tuberculosis* H37Rv, the *OXSR1* knockdown-mediated reduction in *M. tuberculosis* CFU observed at 3 dpi was ameliorated by treatment with the

NLRP3 inhibitor MCC950 (Figure 5D). Supernatant IL-1β was significantly higher in media from *OXSR1* knockdown cells compared to the WT THP-1 cells after *M. tuberculosis* H37Rv infection and this increase in IL-1β was ablated by MCC950 treatment (Figure 5E). Together these data indicate that infection-induced increased expression of *oxsr1a* increases the mycobacterial burden through suppression of inflammasome activation.

Infection-induced OXSR1 suppresses host protective TNF-α and cell death early in infection. Inflammasome-mediated IL-1β increases the macrophage killing of mycobacteria through upregulation of TNF-α[2]. We therefore repeated our infection experiments in *TgBAC(tnfa:GFP)*^{pd1028} embryos to determine if increased TNF-α production was mediating the resistance to mycobacterial infection in *oxsr1a* knockdown zebrafish. The ratio of *tnfa* promoter activity driven GFP per mycobacteria was increased specifically at sites of infection in *oxsr1a* knockdown embryos (Figure 6A) and also in Compound B-treated embryos (Figure 6B). This effect was dependent on *il1b* expression as knockdown of *il1b* suppressed *TgBAC(tnfa:GFP)*^{pd1028}-driven GFP expression around sites of infection (Figure 6C).

To determine if *tnfa* expression acts downstream of *oxsr1a* depletion, we knocked down *tnfa* expression with CRISPR-Cas9 in the *TgBAC(tnfa:GFP)*^{pd1028} background to monitor knockdown efficacy (Figure 6D) [32]. Knockdown of *tnfa* reduced the amount of infection-induced *tnfa* promoter-driven GFP produced around sites of infection and ameliorated the protective effect of *oxsr1a* knockdown against *M. marinum* infection (Figure 6E). Together these data suggest increased TNF-α downstream of inflammasome-processed IL-1β is the mechanism driving the lower bacterial burden in *oxsr1a* knockdown embryos.

Discussion

Here we used the zebrafish-*M. marinum* and *in vitro* human-*M. tuberculosis* experimental systems to show that the WNK-OSXR1 signalling pathway has a critical role in infection-induced activation of the inflammasome. We present evidence that pathogenic mycobacteria increase macrophage K^+ concentration by inducing expression of OXSR1. Infection-induced OXSR1 suppresses protective NLRP3 inflammasome responses and downstream IL-1β/ TNF-α production. Several studies have suggested that mycobacteria modulate inflammasome activation either by active inhibition or by upregulation of NOS, IFN-β and other negative inflammasome regulators[10]. Our data expand this literature by showing that mycobacterial infection-induced OXSR1 expression reduces protective inflammasome activation.

In our infection model we found that WT, but not a-virulent ΔESX1, *M. marinum* induced expression of both OXSR1 and SPAK. The ESX1 secretion system is essential for the virulence of *M. marinum* and is required for escape of the mycobacteria into the cytoplasm [33,34]. This suggests that SPAK/OXSR1 upregulation is driven by the bacteria and fits with the well-established paradigm that pathogenic mycobacteria co-opt host pathways to establish persistent infection[35-39].

We found *stk39* knockdown had no effect on host control of mycobacterial infection in zebrafish embryos. Previous studies have shown that mouse SPAK can play a role in activating macrophage inflammation in both lung injury and inflammatory bowel disease models[40-42]. These data raise the possibility that SPAK and OXSR1 may have species or organ specific roles in innate immunity and may respond differently to sterile and infectious triggers of inflammation.

The effect of Compound B on mycobacterial growth showed that small-molecule inhibition of OXSR1 can reproduce the impact of OXSR1 knockdown on mycobacterial survival. This observation provides proof of concept that OXSR1 may be a suitable target for host-directed therapies against mycobacterial and other intracellular infections. The reduction in bacterial burden was not as large in CB-treated fish as the reduction observed in OXSR1 knockdown embryos. This result may be because the maximum tolerated dose of CB was 1.8 µM, which is low compared to some reported EC_{50} values[30]. Therefore, CB may not have reduced OXSR1 activity to the same extent as in the OXSR1 knockdown embryos.

The results from the THP-1-derived macrophages confirm that the role of OXSR1 in the host response to infection is conserved across species. We showed that infection with WT *M. marinum* decreased the K^+ content of OXSR1 knockdown cells but did not significantly affect the K^+ content of WT cells. Paired with our data showing that WT *M. marinum* increases expression of *oxsr1a*, this suggests that virulent mycobacteria manipulate the SPAK/OXSR1 pathway to maintain high intracellular K^+.

Several studies have shown that K^+ concentration can affect mycobacterial growth and dormancy, and that successful colonisation of macrophages relies on the ability of the bacteria to maintain K^+ homeostasis[43-45]. While here we have examined the effects of K^+ efflux on inflammasome activation, it is possible that the high K^+ maintained in WT cells also aids mycobacterial growth by helping the bacteria maintain the correct ion homeostasis. The mycobacterial infections in THP-1-derived macrophages revealed that both OXSR1 knockdown and treatment with CB resulted in reduced growth of both *M. marinum* and *M.*

241 *tuberculosis* H37Rv in the human macrophage cell line. With *M. marinum* the maximum
242 reduction was observed at 1 dpi, whereas with *M. tuberculosis* this was not seen until 3 days
243 post infection. This is likely to be due to the differing replication times of both pathogens,
244 which are 7 hours and 24 hours, respectively.
245
246 Here we have shown that OXSR1 knockdown can only reduce bacterial burden in zebrafish
247 embryos if NLRP3, IL-1β, and TNFα are functional. In human cells we have shown that infected
248 OXSR1 knockdown cells release significantly more IL-1β into the supernatant and that this is
249 ablated by the NLRP3 inhibitor MCC950. Together this suggests that OXSR1 knockdown
250 reduces bacterial burden via a first step of NLRP3 activation. Previous work in the zebrafish-
251 *M. marinum* model has shown both host detrimental and host beneficial effects of
252 inflammasome activation. While morpholino knockdown of *il1b* has been reported to
253 increase bacterial burden, suggesting that *il1b* plays a host protective role; morpholino
254 knockdown of *caspa* reduced bacterial burden, suggesting caspase-associated cell death of
255 infected macrophages benefits the bacteria [46]. In our experiments we did not find any effect
256 of *il1b* or *nlrp3* knockdown on bacterial burden compared to control embryos. This may have
257 been because we were using mosaic F0 CRISPR knockout, which is not a complete removal or
258 because of *M. marinum* strain differences between studies.
259
260 We found either CB treatment and *oxsr1a* knockdown result in localised increased TNFα
261 production at sites of infection. The fact that we only observed increased TNFα localised to
262 sites of infection, and not throughout the whole embryo, suggests that *oxsr1a* knockdown
263 primes cells for NLRP3 activation but does not cause excess systemic inflammation. Full
264 activation of NLRP3 requires both a priming signal, to induce transcription of NLRP3

components, and pro- IL-1β and an activation signal, to induce oligomerization of NLRP3[18,19]. K^+ efflux should provide only the second signal[18,23]; therefore in cells which have not been primed by infection with bacteria we would not expect to see significant NLRP3 activation. This suggests that OXSR1 inhibition may be an effective host-directed therapy strategy that induces beneficial inflammation at sites of infection without inducing detrimental systemic inflammation.

Our findings that OXSR1 can be targeted to decrease bacterial burden define a new avenue for the development of host-directed therapy. Although numerous studies have investigated the potential of inhibiting NLRP3 to minimize pathology [47], the possibility of activating inflammasomes to increase pathogen clearance has been largely unexplored. Here we have shown that enhancing inflammasome activation via K^+ efflux can provide the dual benefits of maximising the anti-pathogen effects of inflammation without causing excess tissue damage. Given mycobacteria are not the only pathogens which inhibit inflammasome activation, OXSR1 inhibition may be an effective host-directed therapy with broad applicability.

Methods

Zebrafish husbandry

Adult zebrafish were housed at the Centenary Institute (Sydney Local Health District AWC Approval 2017-036). Zebrafish embryos were obtained by natural spawning and embryos were raised at 28°C in E3 media.

Zebrafish lines

289 Wild type zebrafish are the TAB background. Transgenic line was *Tg(tnfa:GFP)*^{pd1028} [48].

290

291 *Infection of zebrafish embryos*

292 Embryos were infected by microinjection with ~400 fluorescent *M. marinum* M strain and
293 ΔESX1 *M. marinum* as previously described[49]. Embryos were recovered into E3 supplemented
294 with 0.036 g/L PTU, housed at 28 °C and imaged on day 5 of infection unless otherwise stated.

295

296 *Quantitative Reverse Transcription PCR (qRT-PCR)*

297 RNA was extracted from 5-10 embryos using TRIzol (Invitrogen) according to the
298 manufacturer's instructions. Equal amounts of RNA (either 1 or 2 µg depending on RNA yield)
299 were used for the cDNA synthesis reaction. qRT-PCR reactions were carried out on a Biorad
300 CFX machine using ThermoFisher PowerUP SYBR green and primers described in Table 1. The
301 relative quantity of transcripts was calculated by the Delta-delta CT method.

302

303 *Imaging*

304 Live zebrafish embryos were anaesthetized in M-222 (Tricaine) and mounted in 3%
305 methylcellulose for static imaging on a Leica M205FA fluorescence stereomicroscope.
306 Fluorescent pixel count analyses were carried out with Image J Software Version 1.51j and
307 intensity measurements were performed as previously described[49].

308

309 *CRISPR-Cas9 knockdown and mutant generation*

310 Primers used for gRNA transcription are detailed in Table 2 and were designed by Wu et al.
311 [50]. Templates for gRNA transcription were produced by annealing and amplifying gene specific

oligos to the scaffold oligo using the NEB Q5 polymerase. Pooled transcription of gRNAs was carried out using the NEB HiScribe T7 High Yield RNA Synthesis Kit.

Embryos were injected at the single cell stage with an injection mix containing 1 µl phenol red, 2 µl 500 ng/µl pooled guides, and 2 µl of 10 µM Cas9. All 'Scram' embryos are injected with scrambled guide RNA.

To create oxsr1a knockout line, F0 crispants were outcrossed to WT AB, and HRM analysis was conducted on F1 progeny. F1s with a visible HRM shift using primers amplifying the 4 predicted cut sites (primer 3 spanned 2 cut sites) were sent for sanger sequencing. An F1 was discovered carrying an 8 bp deletion causing a premature stop at amino acid 13 (Extended Data 2). F2 progeny were genotyped with a custom KASP assay ordered from LGC Biosearch Technologies.

Drug treatments

Embryos and cells were treated with vehicle control (DMSO or water as appropriate), 10 µM MCC950, 77 µM Ac-YVAD-cmk, 1.8 µM Compound B, or 48 µM Furosemide (Sigma) immediately after infection. For zebrafish, the drugs and E3 were replaced on days 0, 2, and 4 dpi. For cell culture, drugs were replaced at 4 hours post infection.

Axenic culture

A mid-log culture of fluorescent *M. marinum* was diluted 1:100 and aliquoted into 96 well plates for drug treatment. Cultures were maintained at 28°C in a static incubator and bacterial fluorescence was measured in a BMG Fluorostar plate reader.

THP-1 cell culture

Human THP-1 cells (ATCC® TIB-202™) were cultured in RPMI media (22400089, ThermoFisher) supplemented with 1% (v/v) non-essential amino acids (11140050, ThermoFisher), 1 mM sodium pyruvate (11360070, ThermoFisher), 10% (v/v) FCS (Hyclone, GE Healthcare) and 0.1 mg/ml penicillin/streptomycin (15140122, ThermoFisher) at 37°C, 5% CO_2.

Viral production

24 hours prior to transfection, $4x10^6$ HEK2937 cells were seeded in a 100 mm culture dish. On the day of transfection, cells were co-transfected with 15ug of the pLKO.1_GFP (#30323, Addgene) vector containing OXSR1_Sh1, OXSR1_Sh2 or AthmiR, 6.5 µg of the packaging plasmid pMDL-g/prre (#12251, Addgene), 2.5 µg of the packaging plasmid pRSV-Rev (#12253, Addgene) and 3.5 µg of the envelop expressing plasmid pMD2-VSV-G (#12259, Addgene) by the calcium phosphate transfection method. Culture media was changed the following day and cells were cultured for another 24 hours. Medium containing lentiviral particles was then collected, debris was cleared by centrifugation at 430 g for 5 minutes, filtered through a 0.45 µm filter, aliquoted, and stored at -80°C.

Transduction

Briefly, $5x10^5$ THP-1 cells were resuspended in 500 µl of fresh culture media containing 10 µg/ml polybrene. After adding 50 µl of virus, cells were spinoculated for 90 min at 462 g, 22°C. After spinning, pelleted cells were resuspended in in the same media and incubated for 4 hours at 37C, 5%CO2. Following incubation, cells were pelleted, resuspended in fresh culture

359 media and transferred to a 6 well plate. Cells were cultured for 48 hours before FACS
360 selection.
361
362 *Western Blotting*
363 Protein lysates were loaded onto 4-12% BIS-Tris Protein gels (NP0336BOX, ThermoFisher) for
364 electrophoresis followed by transfer onto a PVDF membrane (MILIPVH00010, Merck
365 Millipore). Membrane was blocked with 5% (v/v) skim milk for 1 hour at room temperature,
366 incubated overnight with a 1:1000 dilution of rabbit anti-OXSR1 (ab97694, Abcam) followed
367 by incubation with a 1:5000 dilution of a donkey anti-rabbit IgG HRP antibody (AP182P, Merck
368 Millipore) and 1:5000 dilution of mouse anti-GAPDH (ab8245, Abcam) antibody, followed by
369 incubation with a 1:5000 dilution of a donkey anti-mouse IgG HRP antibody (AP192P, Merck
370 Millipore). Protein detection was performed using SuperSignal West Pico PLUS (34579,
371 ThermoFisher) and imaged on a Bio-Rad ChemiDoc Imaging System.
372
373 *ION K+ Green (undifferentiated cells)*
374 For flow cytometry, $2x10^5$ undifferentiated THP-1 cells/well (ATCC® TIB-202™) were seeded
375 into a 96 well plate and incubated at 37°C for 1.5-2 hrs with either Furosemide, 37.5 mM or
376 75 mM KCl. ION K+ Green was added to a final concentration of 52.8 mM and cells were
377 incubated for a further 15 minutes. Cells were spun down for 5 minutes at 462 g and
378 resuspended in PBS + 2% FCS supplemented with either Furosemide, 37.5 mM or 75 mM KCl.
379 ION K+ Green fluorescence was captured on a BD Fortessa through the PE channel. 5000
380 events were captured per sample.
381
382 *ION K+ Green (differentiated cells)*

$2x10^5$ THP-1 cells/well were seeded into a 96 well plate and differentiated for 24 hrs with 100 mM PMA. Cells were then infected with frozen single cell preparation *M. marinum*-katushka at an MOI of 1. After 4 hrs extracellular bacteria were removed by washing with PBS + 2% FCS, and cells were incubated at 32°C for 3 days. Cells were lifted from the plate by 15 minute incubation at 37°C with Accutase™ (StemCell Technologies), then washed with PBS + 2% FCS. ION K+ Green was added to a final concentration of 52.8 mM and cells were incubated for a further 15 minutes. Cells were spun down for 5 minutes at 462 g and resuspended in PBS + 2% FCS for flow cytometry. ION K+ Green fluorescence was captured on a BD Fortessa through the FITC channel (so as not to overlap with katushka). 5000 events were captured per sample.

For static imaging, THP-1 cells were seeded onto an imaging slide coated with 1% low melting point agarose and differentiated for 24 hrs with 100 mM PMA. ION K+ Green was added to a final concentration of 52.8 mM and cells were incubated for 15 minutes at 37°C. Culture media was replaced with PBS + 2% FCS. Cells were imaged on a Leica Sp8 and mean ION K+ Green fluorescence was analysed using the 'measure' function in Image J.

Mycobacterial infection of THP-1 cells

$2x10^5$ THP-1 cells/well were seeded into a 96 well plate and differentiated for 24 hrs with 100 mM PMA. Cells were then infected with either mid log culture of *M. tuberculosis* H37Rv or frozen single cell preparation of *M. marinum* at an MOI of 1. After 4 hrs, extracellular bacteria were removed by washing with PBS + 2% FCS, and cells were incubated at either 32°C for *M. marinum* infections or 37°C for *M. tuberculosis* infections.

Mycobacterial CFU recovery from THP-1 cells

Cells were washed in PBS + 2% FCS and lysed with TDW + 1% Triton X100 for 10 minutes. lysate was serially diluted and plated on 7H10 agar supplemented with 50 µg/ml hygromycin for the recovery of *M. marinum* or a mix of 200,000 units/L polymyxin B, 50mg/L carbenicillin, 10mg/L amphotericin B, and 20mg/L trimethoprim lactate for the recovery of *M. tuberculosis*. Plates were incubated at 32°C for 7 days (*M. marinum*) or 37°C for 14 days (*M. tuberculosis).*

Measurement of human IL-1β in supernatants

IL-1β was measured by cytometric bead array, using a human IL-1β enhanced-sensitivity flex set (BD Biosciences). Undiluted cell supernatant was stained according to the manufacturer's instructions and run on a BD FACS Canto II. Data was analysed using FCAP array software.

Statistics

All statistical tests were calculated in Graphpad Prism. T-tests were unpaired t-tests with Welch's correction. All ANOVA were ordinary one-way ANOVA, comparing the means of specified pairings, using Turkey's multiple comparisons test with a single pooled variance. In cases where data was pooled from multiple experiments, data from each was normalized to its own within-experiment control (usually DMSO) before pooling. Error bars indicate SEM. Outliers were removed using ROUT, with Q=1%.

Funding

This work was supported by the Australian National Health and Medical Research Council [grant numbers APP1099912, APP1053407 to S.H.O.; APP1153493 to W.J.B.]; University of Sydney Fellowship [grant number G197581 to S.H.O.]; NSW Ministry of Health under the NSW Health Early-Mid Career Fellowships Scheme [grant number H18/31086 to S.H.O.]; the

Kenyon Family Inflammation Award [2019 to E.H.] and the Centenary Institute Booster Grant [2020 to E.H.].

Acknowledgements

We thank Dr Kristina Jahn of Sydney Cytometry for assistance with imaging equipment; Ms Kaiming Luo and Dr Pradeep Cholan for technical assistance, and all members of the Tuberculosis Research Program at the Centenary Institute for helpful comments.

Author contributions

E.H. and S.H.O designed the experiments. E.H., V.L.T, S.H.O. performed the experiments. A.R.M.F. performed microscopy. N.P. and J.J-L.W. generated knockdown cell lines. E.H. and S.O. wrote the paper that was reviewed by all authors. W.J.B., and S.H.O. supervised the project.

Declaration of Interests

The authors declare no competing interests.

References

1 Wawrocki, S. & Druszczynska, M. Inflammasomes in Mycobacterium tuberculosis-Driven Immunity. *Can J Infect Dis Med Microbiol* **2017**, 2309478, doi:10.1155/2017/2309478 (2017).

2 Jayaraman, P. *et al.* IL-1beta promotes antimicrobial immunity in macrophages by regulating TNFR signaling and caspase-3 activation. *J Immunol* **190**, 4196-4204, doi:10.4049/jimmunol.1202688 (2013).

3 Taxman, D. J., Huang, M. T. & Ting, J. P. Inflammasome inhibition as a pathogenic stealth mechanism. *Cell Host Microbe* **8**, 7-11, doi:10.1016/j.chom.2010.06.005 (2010).

4 Lu, A. & Wu, H. Structural mechanisms of inflammasome assembly. *FEBS J* **282**, 435-444, doi:10.1111/febs.13133 (2015).

5 Master, S. S. *et al.* Mycobacterium tuberculosis prevents inflammasome activation. *Cell Host Microbe* **3**, 224-232, doi:10.1016/j.chom.2008.03.003 (2008).

6 Sousa, J. *et al.* Mycobacterium tuberculosis associated with severe tuberculosis evades cytosolic surveillance systems and modulates IL-1beta production. *Nat Commun* **11**, 1949, doi:10.1038/s41467-020-15832-6 (2020).

7 Koo, I. C. *et al.* ESX-1-dependent cytolysis in lysosome secretion and inflammasome activation during mycobacterial infection. *Cell Microbiol* **10**, 1866-1878, doi:10.1111/j.1462-5822.2008.01177.x (2008).

8 Kurenuma, T. *et al.* The RD1 locus in the Mycobacterium tuberculosis genome contributes to activation of caspase-1 via induction of potassium ion efflux in infected macrophages. *Infect Immun* **77**, 3992-4001, doi:10.1128/IAI.00015-09 (2009).

9 Dorhoi, A. *et al.* Activation of the NLRP3 inflammasome by Mycobacterium tuberculosis is uncoupled from susceptibility to active tuberculosis. *Eur J Immunol* **42**, 374-384, doi:10.1002/eji.201141548 (2012).

10 Briken, V., Ahlbrand, S. E. & Shah, S. Mycobacterium tuberculosis and the host cell inflammasome: a complex relationship. *Front Cell Infect Microbiol* **3**, 62, doi:10.3389/fcimb.2013.00062 (2013).

11 Carlsson, F. *et al.* Host-detrimental role of Esx-1-mediated inflammasome activation in mycobacterial infection. *PLoS Pathog* **6**, e1000895, doi:10.1371/journal.ppat.1000895 (2010).

12 Mishra, B. B. *et al.* Nitric oxide controls the immunopathology of tuberculosis by inhibiting NLRP3 inflammasome-dependent processing of IL-1beta. *Nat Immunol* **14**, 52-60, doi:10.1038/ni.2474 (2013).

13 Li, Q. *et al.* Heme induces IL-1beta secretion through activating NLRP3 in kidney inflammation. *Cell Biochem Biophys* **69**, 495-502, doi:10.1007/s12013-014-9823-9 (2014).

14 Erdei, J. *et al.* Induction of NLRP3 Inflammasome Activation by Heme in Human Endothelial Cells. *Oxid Med Cell Longev* **2018**, 4310816, doi:10.1155/2018/4310816 (2018).

15 Greaney, A. J., Leppla, S. H. & Moayeri, M. Bacterial Exotoxins and the Inflammasome. *Frontiers in immunology* **6**, 570, doi:10.3389/fimmu.2015.00570 (2015).

16 Eigenbrod, T. & Dalpke, A. H. Bacterial RNA: An Underestimated Stimulus for Innate Immune Responses. *J Immunol* **195**, 411-418, doi:10.4049/jimmunol.1500530 (2015).

17 Gupta, R. *et al.* RNA and beta-hemolysin of group B Streptococcus induce interleukin-1beta (IL-1beta) by activating NLRP3 inflammasomes in mouse macrophages. *J Biol Chem* **289**, 13701-13705, doi:10.1074/jbc.C114.548982 (2014).

18 Kelley, N., Jeltema, D., Duan, Y. & He, Y. The NLRP3 Inflammasome: An Overview of Mechanisms of Activation and Regulation. *Int J Mol Sci* **20**, doi:10.3390/ijms20133328 (2019).

19 He, Y., Hara, H. & Nunez, G. Mechanism and Regulation of NLRP3 Inflammasome Activation. *Trends Biochem Sci* **41**, 1012-1021, doi:10.1016/j.tibs.2016.09.002 (2016).

20 Perregaux, D. & Gabel, C. A. Interleukin-1 beta maturation and release in response to ATP and nigericin. Evidence that potassium depletion mediated by these agents is a necessary and common feature of their activity. *J Biol Chem* **269**, 15195-15203 (1994).

21 Petrilli, V. *et al.* Activation of the NALP3 inflammasome is triggered by low intracellular potassium concentration. *Cell Death Differ* **14**, 1583-1589, doi:10.1038/sj.cdd.4402195 (2007).

22 Franchi, L., Kanneganti, T. D., Dubyak, G. R. & Nunez, G. Differential requirement of P2X7 receptor and intracellular K+ for caspase-1 activation induced by intracellular and extracellular bacteria. *J Biol Chem* **282**, 18810-18818, doi:10.1074/jbc.M610762200 (2007).

23 Munoz-Planillo, R. *et al.* K(+) efflux is the common trigger of NLRP3 inflammasome activation by bacterial toxins and particulate matter. *Immunity* **38**, 1142-1153, doi:10.1016/j.immuni.2013.05.016 (2013).

24 Meng, G., Zhang, F., Fuss, I., Kitani, A. & Strober, W. A mutation in the Nlrp3 gene causing inflammasome hyperactivation potentiates Th17 cell-dominant immune responses. *Immunity* **30**, 860-874, doi:10.1016/j.immuni.2009.04.012 (2009).

25 Gagnon, K. B. & Delpire, E. Molecular physiology of SPAK and OSR1: two Ste20-related protein kinases regulating ion transport. *Physiol Rev* **92**, 1577-1617, doi:10.1152/physrev.00009.2012 (2012).

26 Brown, F. C. *et al.* Activation of the erythroid K-Cl cotransporter Kcc1 enhances sickle cell disease pathology in a humanized mouse model. *Blood* **126**, 2863-2870, doi:10.1182/blood-2014-10-609362 (2015).

27 Hortle, E. *et al.* KCC1 Activation protects Mice from the Development of Experimental Cerebral Malaria. *Scientific reports* **9**, 6356, doi:10.1038/s41598-019-42782-x (2019).

28 Rougeot, J. *et al.* Corrigendum: RNAseq Profiling of Leukocyte Populations in Zebrafish Larvae Reveals a cxcl11 Chemokine Gene as a Marker of Macrophage Polarization During Mycobacterial Infection. *Frontiers in immunology* **10**, 2720, doi:10.3389/fimmu.2019.02720 (2019).

29 Ishigami-Yuasa, M. *et al.* Development of WNK signaling inhibitors as a new class of antihypertensive drugs. *Bioorg Med Chem* **25**, 3845-3852, doi:10.1016/j.bmc.2017.05.034 (2017).

30 Mori, T. *et al.* Chemical library screening for WNK signalling inhibitors using fluorescence correlation spectroscopy. *Biochem J* **455**, 339-345, doi:10.1042/BJ20130597 (2013).

31 Smith, J. *et al.* Evidence for pore formation in host cell membranes by ESX-1-secreted ESAT-6 and its role in Mycobacterium marinum escape from the vacuole. *Infect Immun* **76**, 5478-5487, doi:10.1128/IAI.00614-08 (2008).

32 Hortle, E. *et al.* Rough and smooth variant Mycobacterium abscessus infections are differentially controlled by host immunity during chronic infection of adult zebrafish. *Nat Commun*, doi: https://doi.org/10.1101/856948 (2021).

33 Conrad, W. H. *et al.* Mycobacterial ESX-1 secretion system mediates host cell lysis through bacterium contact-dependent gross membrane disruptions. *Proc Natl Acad Sci U S A* **114**, 1371-1376, doi:10.1073/pnas.1620133114 (2017).

34 Lienard, J. *et al.* The Mycobacterium marinum ESX-1 system mediates phagosomal permeabilization and type I interferon production via separable mechanisms. *Proc Natl Acad Sci U S A* **117**, 1160-1166, doi:10.1073/pnas.1911646117 (2020).

35 Hortle, E. *et al.* Thrombocyte inhibition restores protective immunity to mycobacterial infection in zebrafish. *J Infect Dis*, doi:10.1093/infdis/jiz110 (2019).

36 Oehlers, S. H. *et al.* Infection-induced vascular permeability aids mycobacterial growth. *J Infect Dis* **215**, 813-817, doi:10.1093/infdis/jiw355 (2017).

37 Oehlers, S. H. *et al.* Interception of host angiogenic signalling limits mycobacterial growth. *Nature* **517**, 612-615, doi:10.1038/nature13967 (2015).

38 Johansen, M. D. *et al.* Mycobacterium marinum infection drives foam cell differentiation in zebrafish infection models. *Dev Comp Immunol* **88**, 169-172, doi:10.1016/j.dci.2018.07.022 (2018).

39 Hortle, E. & Oehlers, S. H. Host-directed therapies targeting the tuberculosis granuloma stroma. *Pathogens and disease* **78**, doi:10.1093/femspd/ftaa015 (2020).

40 Hung, C. M., Peng, C. K., Yang, S. S., Shui, H. A. & Huang, K. L. WNK4-SPAK modulates lipopolysaccharide-induced macrophage activation. *Biochem Pharmacol* **171**, 113738, doi:10.1016/j.bcp.2019.113738 (2020).

41 Yan, Y. *et al.* Overexpression of Ste20-related proline/alanine-rich kinase exacerbates experimental colitis in mice. *J Immunol* **187**, 1496-1505, doi:10.4049/jimmunol.1002910 (2011).

42 Zhang, Y. *et al.* Knockout of Ste20-like proline/alanine-rich kinase (SPAK) attenuates intestinal inflammation in mice. *Am J Pathol* **182**, 1617-1628, doi:10.1016/j.ajpath.2013.01.028 (2013).

43 Steel, H. C., Matlola, N. M. & Anderson, R. Inhibition of potassium transport and growth of mycobacteria exposed to clofazimine and B669 is associated with a calcium-independent increase in microbial phospholipase A2 activity. *The Journal of antimicrobial chemotherapy* **44**, 209-216, doi:10.1093/jac/44.2.209 (1999).

44 MacGilvary, N. J., Kevorkian, Y. L. & Tan, S. Potassium response and homeostasis in Mycobacterium tuberculosis modulates environmental adaptation and is important for host colonization. *PLoS Pathog* **15**, e1007591, doi:10.1371/journal.ppat.1007591 (2019).

45 Salina, E. G. *et al.* Potassium availability triggers Mycobacterium tuberculosis transition to, and resuscitation from, non-culturable (dormant) states. *Open Biol* **4**, doi:10.1098/rsob.140106 (2014).

46 Varela, M., van der Vaart, M., Groenewoud, A. & Meijer, A. H. Extracellular mycobacterial DNA drives disease progression by triggering Caspase-11-dependent pyroptosis of infected macrophages. *bioRxiv*, 514125, doi:10.1101/514125 (2019).

47 Yang, Y., Wang, H., Kouadir, M., Song, H. & Shi, F. Recent advances in the mechanisms of NLRP3 inflammasome activation and its inhibitors. *Cell Death Dis* **10**, 128, doi:10.1038/s41419-019-1413-8 (2019).

48 Marjoram, L. *et al.* Epigenetic control of intestinal barrier function and inflammation in zebrafish. *Proc Natl Acad Sci U S A* **112**, 2770-2775, doi:10.1073/pnas.1424089112 (2015).

49 Matty, M. A., Oehlers, S. H. & Tobin, D. M. Live Imaging of Host-Pathogen Interactions in Zebrafish Larvae. *Methods Mol Biol* **1451**, 207-223, doi:10.1007/978-1-4939-3771-4_14 (2016).

50 Wu, R. S. *et al.* A Rapid Method for Directed Gene Knockout for Screening in G0 Zebrafish. *Dev Cell* **46**, 112-125 e114, doi:10.1016/j.devcel.2018.06.003 (2018).

Figures

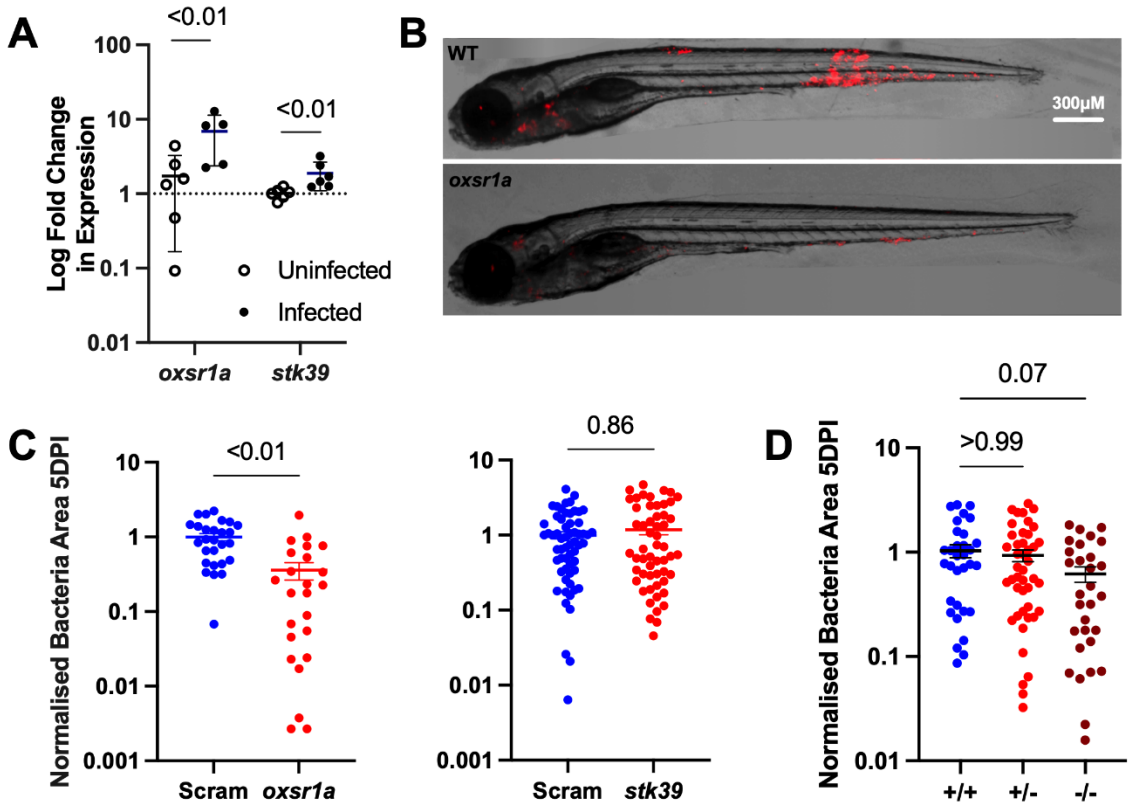

Figure 1: Infection-induced OXSR1 aids the growth of *M. marinum* in zebrafish.

A) Relative expression of *oxsr1a* and *stk39* in 3 dpi *M. marinum*-infected zebrafish embryos, compared to matched uninfected controls. Biological replicates (n=6) each represent pooled RNA from 7-10 embryos. B) Representative images of *M.* marinum-tdTomato (red) bacterial burden in scramble control and mosaic F0 *oxsr1a* crispant embryos. C) Quantification of *M. marinum* bacterial burden in scramble control, mosaic F0 *oxsr1a* and *stk39* crispant embryos. Each graph shows combined results of two independent experiments. D) Quantification of *M. marinum* bacterial burden in WT, heterozygous and homozygous *oxsr1a* knockout embryos. Graph shows combined results of two independent experiments.

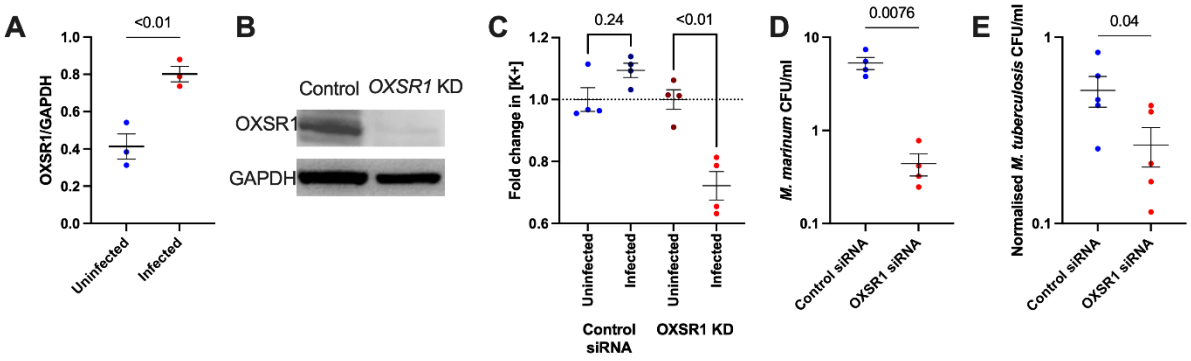

606

607 **Figure 2: OXSR1 aids the growth of *M. tuberculosis* in human THP-1 cells.**

608 A) Quantification of OXSR1 protein in *M. tuberculosis*-infected PMA-differentiated THP-1
609 cells. Blots are included in Extended data 3. B) Western blot of *OXSR1* knockdown and vector
610 control THP-1 cell lines, showing loss of OXSR1. Full un-edited blots are included in Extended
611 data 3. C) Fold change of ION K+ green mean fluorescence intensity (measured by flow
612 cytometry) of *M. marinum* infected control and *OXSR1* knockdown THP-1 cells. Fold change
613 was calculated by dividing the MFI of cells positive for *M. marinum*-Katushka by the MFI of
614 cells from the uninfected group. D) Quantification of intracellular *M. marinum* burden in 1
615 dpi *OXSR1* knockdown PMA-differentiated THP-1 cells. E) Quantification of intracellular *M.*
616 *tuberculosis* burden in 3 dpi *OXSR1* knockdown PMA-differentiated THP-1 cells.

617

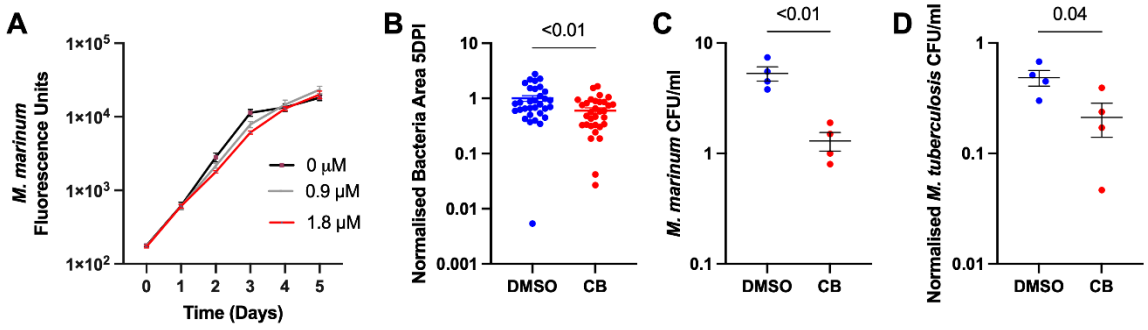

618

619 **Figure 3: Compound B inhibition of SPAK/OXSR1 reduces mycobacterial burden in zebrafish**
620 **embryos and human THP-1 cells.**

621 A) Quantification of axenic *M.* marinum-tdTomato growth by fluorescence in 7H9 broth
622 culture supplemented with Compound B (CB). Red line (1.8 µM) indicates the concentration
623 used to treat infected embryos. B) Quantification of *M. marinum* bacterial burden in CB-
624 treated zebrafish embryos. C) Quantification of intracellular *M. marinum* burden in 1 dpi CB-
625 treated PMA-differentiated THP-1 cells. D) Quantification of intracellular *M. tuberculosis*
626 burden in 3 dpi CB-treated PMA-differentiated THP-1 cells.
627

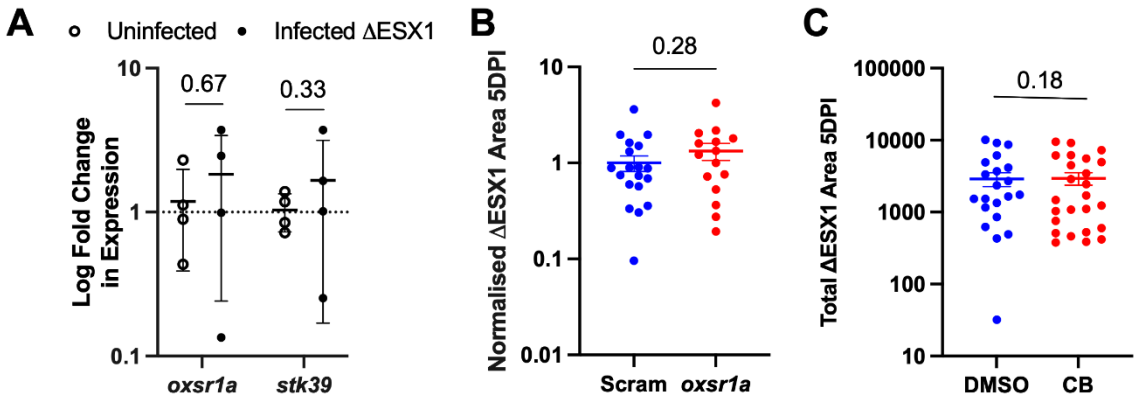

628

629 **Figure 4: *M. marinum* ESX1 drives infection-induced *oxsr1a* expression**

630 A) Relative expression of *oxsr1a* and *stk39* in zebrafish embryos at 3 days post infection with
631 ΔESX1-*M. marinum* compared to age-matched uninfected controls. Biological replicates (n=4)
632 represent pooled RNA from 7-10 embryos. B) Quantification of ΔESX1-*M. marinum* bacterial
633 burden in scramble control and mosaic F0 *oxsr1a* CRISPR embryos. C) Quantification of ΔESX1-
634 *M. marinum* bacterial burden in DMSO vehicle control and Compound B-treated embryos.
635

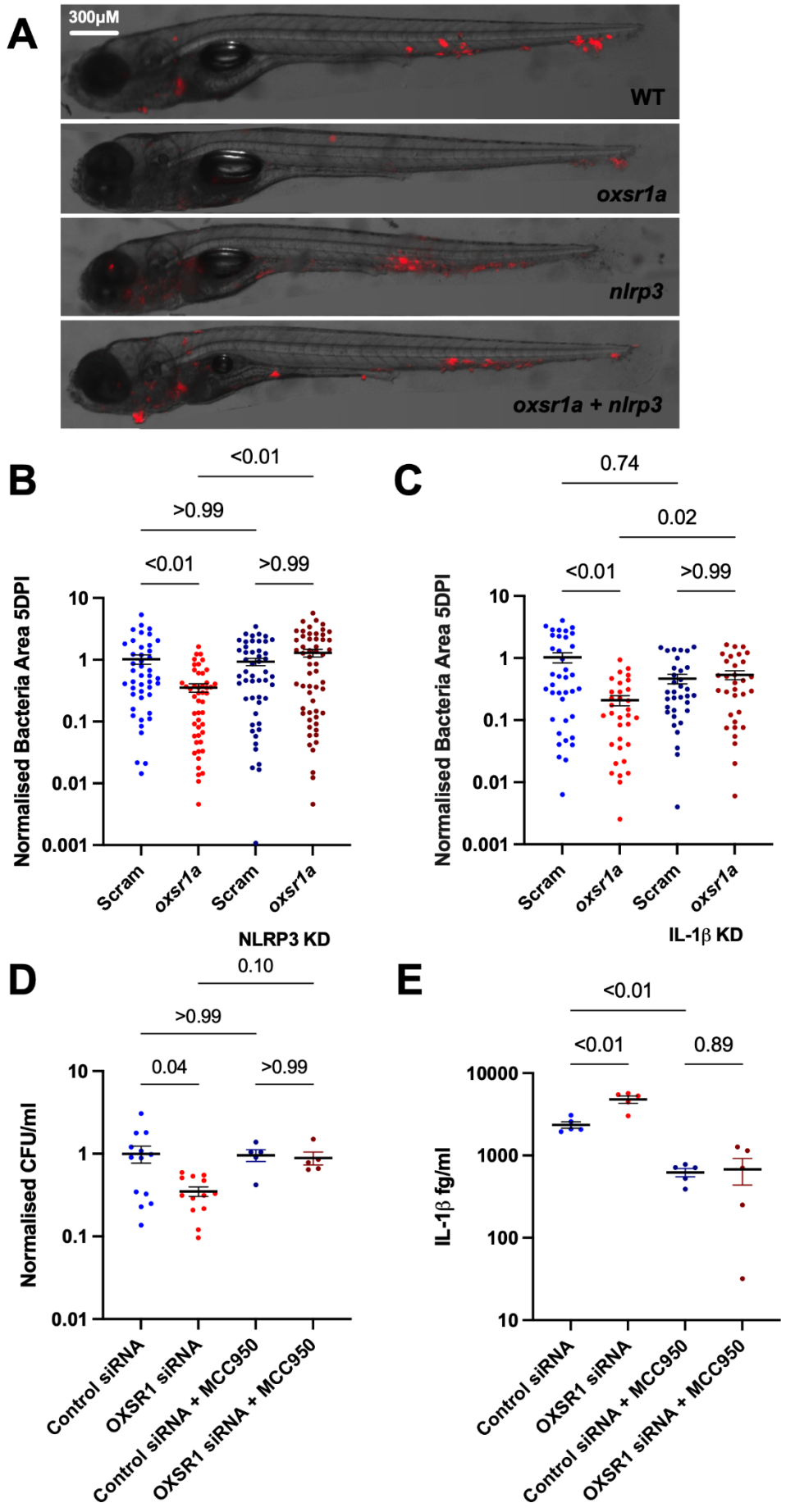

637 **Figure 5: Infection-induced OXSR1 suppresses inflammasome activity to aid mycobacterial**
638 **infection.**

639 A) Representative images of *M. marinum*-tdTomato (red) bacterial burden in 5 dpi WT, mosaic
640 F0 *oxsr1a, nlrp3,* and dual *oxsr1a nlrp3* crispant embryos. Scale bar represents 300 µm. B)
641 Quantification of *M. marinum* bacterial burden in scramble control, mosaic F0 *oxsr1a, nlrp3,*
642 and dual *oxsr1a nlrp3* crispant embryos. Combined results of 3 biological replicates. C)
643 Quantification of *M. marinum* bacterial burden in scramble control, mosaic F0 *oxsr1a, Il1b,*
644 and dual *oxsr1a Il1b* crispant embryos. Combined results of 2 biological replicates. D)
645 Quantification of intracellular *M. tuberculosis* bacterial burden in 3 dpi O*XSR1* knockdown
646 PMA-differentiated THP-1 cells. E) IL-1β content in the supernatant of 3 dpi *M. tuberculosis*-
647 infected O*XSR1* knockdown PMA-differentiated THP-1 cells.

648

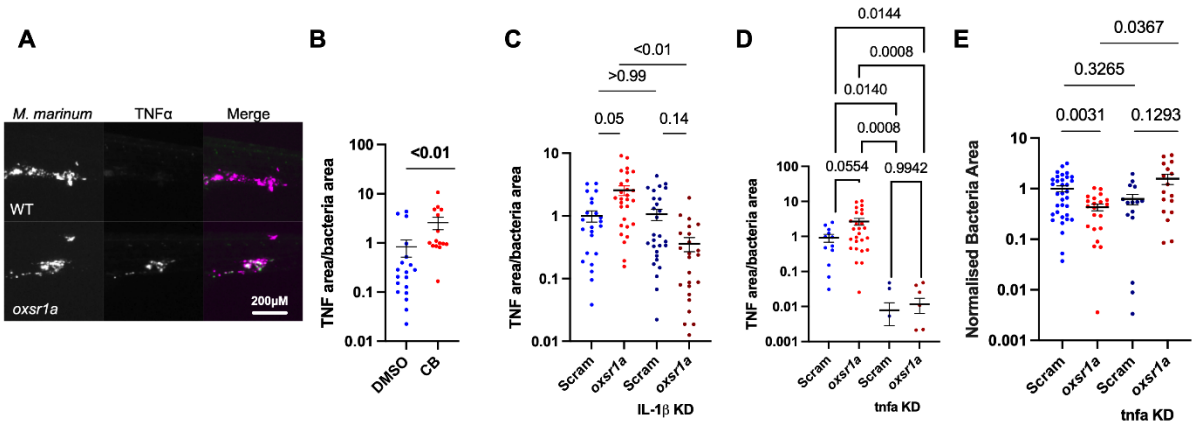

649

650 **Figure 6: Infection-induced OXSR1 suppresses inflammasome activity to aid mycobacterial**
651 **infection.**

652 A) Representative images of *Tg(tnfa:GFP)*^{pd1028} fluorescence around *M. marinum*
653 granulomas. Scale bar represents 200 µm. B) Quantification of *Tg(tnfa:GFP)*^{pd1028}
654 fluorescent pixels per bacterial pixel in *M. marinum*-infected CB-treated zebrafish
655 embryos. C) Quantification of *Tg(tnfa:GFP)*^{pd1028} fluorescent pixels per bacterial pixel

in *M. marinum*-infected WT, mosaic F0 *oxsr1a, Il1b,* and dual *oxsr1a Il1b* crispant embryos. Combined results of 2 independent experiments. D) Quantification of *Tg(tnfa:GFP)*^{pd1028} fluorescent pixels per bacterial pixel in *M. marinum*-infected WT, mosaic F0 *oxsr1a, tnfa,* and dual *oxsr1a tnfa* crispant embryos. Combined results of 2 independent experiments. E) Quantification of *M. marinum* burden in WT, mosaic F0 *oxsr1a, tnfa,* and dual *oxsr1a tnfa* crispant embryos. Combined results of 2 independent experiments.

B)

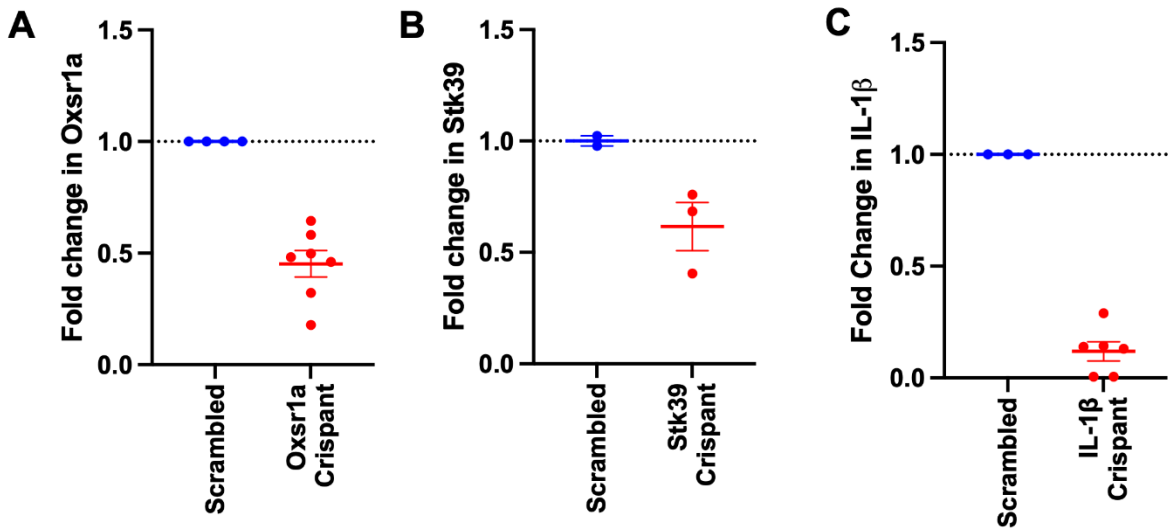

Extended Data 1

Knockdown efficacy for CRISPR-Cas9 depletion of A) *oxsr1a*, B) *stk39*, C) *il1b*, in zebrafish embryos.

A

GTTGGCAAAGTTTGGCTGTTGGGACTGAGAGCGGTCGGTGAGATCAGCAC
AAGTAAATCGAGTATAAATACAGATCGGTCGTTTTCCAGCGCTCGCCGCC
GTGTAAGCGTGCAGTGGGGCGTCCGGCTGTCGTGATCTGACCGCAGTCAT
GTCCGAGGACCCGAGCTCTCAACCTTGGTCCATCGACAAGGATGACTATG
AGCTACAGGAGGTGATCGgtgagctaatccaccacacatcagcatctcaa
tcacacgagtgacagaaaacggagagtaatgcggaggtgtttatatcggt
gtggccctgatgatctgtgttcgttcagatctccatcagtgattgagtca

B

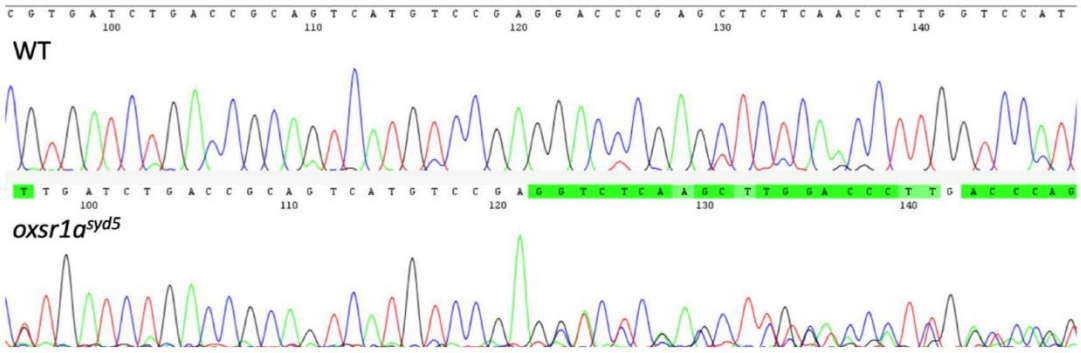

WT: CCGAGGACCCGAGCTCTCAACCTT

oxsr1a^{syd5} : CCGAG--------CTCTCAACCTT

C

WT: MSEDPSSQPWSIDKDDYELQ

oxsr1a^{syd5}: MSELSTLVHRQGStop

D

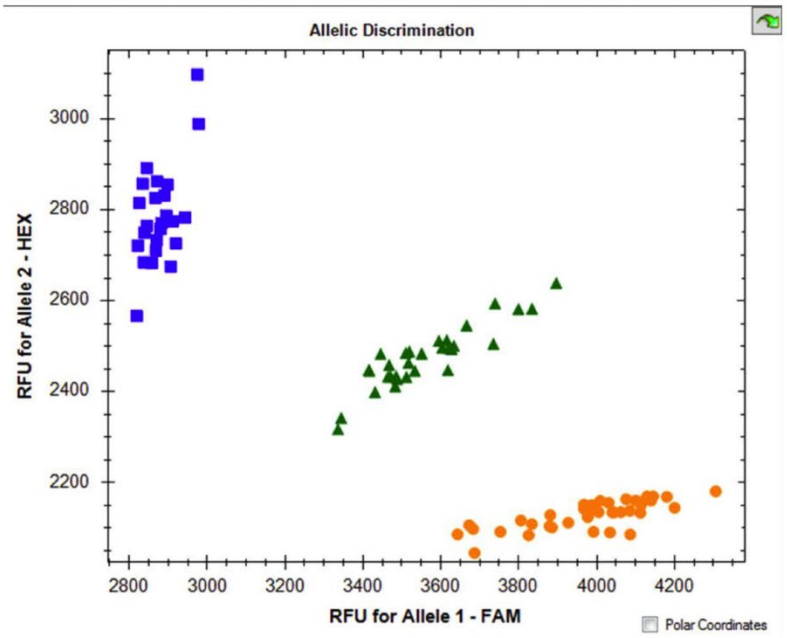

Extended Data 2

Generation of the *oxsr1a*^{syd5} allele.

A) Map of primer binding sites (blue) and gRNA binding site (pink) around the *oxsr1a*^{syd5} allele. Sequence shows exon 1 (upper case) and part of intron 1 (lower case) of *oxsr1a* B) Chromatograms showing partial sequence of the *oxsr1a*^{syd5} allele. C) Predicted OXSR1 protein sequence of the *oxsr1a*^{syd5} allele. D) Representative genotyping results of hetxhet F2 cross. FAM = WT allele; HEX = *oxsr1a*^{syd5} allele.

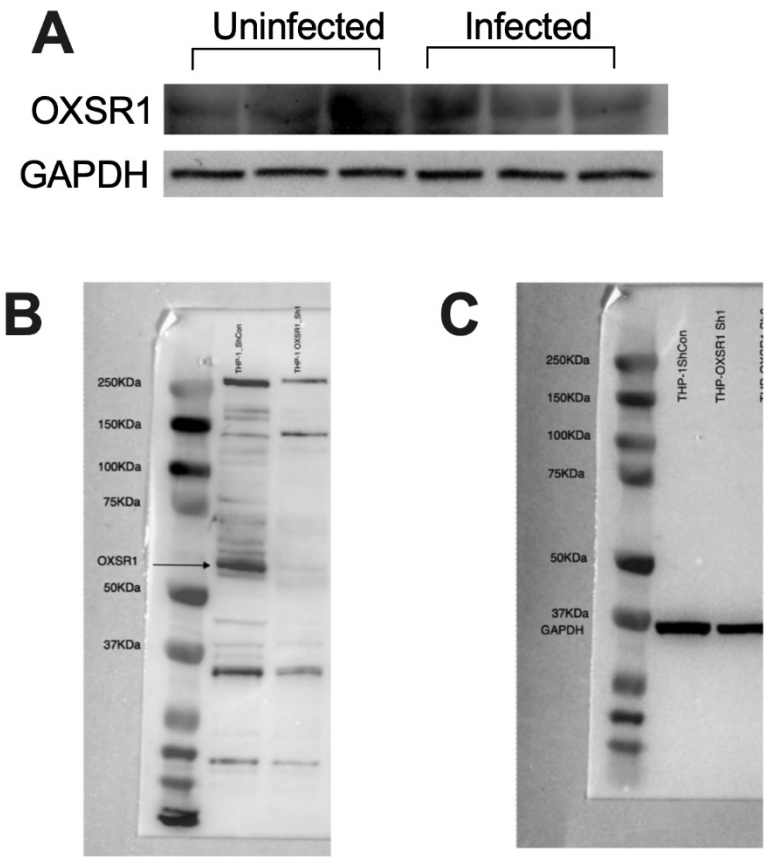

Extended Data 3

A) Western blot of OXSR1 and GAPDH protein levels in 3 dpi PMA-differentiated *M. tuberculosis*-infected THP-1 cells. Full western blots showing OXSR1 (B) and GAPDH (C) protein levels in THP-1 control and knockdown cell lines.

683

684 **Table 1**

685 Primers used for gene expression studies.

686

	Sequence 5‘-3‘
Oxsr1a qFw	gctgctttacggtcaccaag
Oxsr1a qRv	attttagccgagtcctgccc
Stk39 qFw	gatcgcagattttggcgtga
Stk39 qRv	gatatcgatggtacggcgca
EF1a qFw	tgccttcgtcccaatttcag
EF1a qRv	taccctccttgcgctcaatc
IL-1β qFW	atcaaaccccaatccacagagt
IL-1β qRv	ggcactgaagacaccacgtt

687

688 **Table 2**

689 Primers used to generate gRNAs for CRISPR-Cas9 knockdown.

	Sequence 5‘-3‘
il1b_Target_1	TAATACGACTCACTATAGGGTTCAGATCCGCTTGCAAGTTTTAGAGCTAGAAATAGC
il1b_Target_2	TAATACGACTCACTATAGGCATGGCGAACGTCATCCAGTTTTAGAGCTAGAAATAGC
il1b_Target_3	TAATACGACTCACTATAGGCACTGGGCGACGCATACGGTTTTAGAGCTAGAAATAGC
il1b_Target_4	TAATACGACTCACTATAGGCAGCTGGTCGTATCCGTTGTTTTAGAGCTAGAAATAGC
oxsr1a_Target_1	TAATACGACTCACTATAGGGTTGAGAGCTCGGGTCCTGTTTTAGAGCTAGAAATAGC
oxsr1a_Target_2	TAATACGACTCACTATAGGGCACCTCTCTTAGTATGGGTTTTAGAGCTAGAAATAGC
oxsr1a_Target_3	TAATACGACTCACTATAGGTCCAGTCTCTAAACACGGGTTTTAGAGCTAGAAATAGC
oxsr1a_Target_4	TAATACGACTCACTATAGGAGGCGGTGCCGAATGCGGGTTTTAGAGCTAGAAATAGC

scramble_target_1	TAATACGACTCACTATAGGCAGGCAAAGAATCCCTGCCGTTTTAGAGCTAGAAATAGC
scramble_target_2	TAATACGACTCACTATAGGTACAGTGGACCTCGGTGTCGTTTTAGAGCTAGAAATAGC
scramble_target_3	TAATACGACTCACTATAGGCTTCATACAATAGACGATGGTTTTAGAGCTAGAAATAGC
scramble_target_4	TAATACGACTCACTATAGGTCGTTTTGCAGTAGGATCGGTTTAGAGCTAGAAATAGC
si:zfos-364h11.1_Target_1	TAATACGACTCACTATAGGTATAGAGACTCTTTGTACGTTTTAGAGCTAGAAATAGC
si:zfos-364h11.1_Target_2	TAATACGACTCACTATAGGGATCTGATTAGTTGCTGCGTTTTAGAGCTAGAAATAGC
si:zfos-364h11.1_Target_3	TAATACGACTCACTATAGGGCTTCGTCACTGAATTCAGTTTTAGAGCTAGAAATAGC
si:zfos-364h11.1_Target_4	TAATACGACTCACTATAGGAGCTCTCTTAGTGAGTTTGTTTTAGAGCTAGAAATAGC
STK39_Target_1	TAATACGACTCACTATAGGGTAGTAGGTGACCACGTTGTTTTAGAGCTAGAAATAGC
STK39_Target_2	TAATACGACTCACTATAGGGACCTGCTCCATTACTTCGTTTTAGAGCTAGAAATAGC
STK39_Target_3	TAATACGACTCACTATAGGAGAACGATCCTCCCTCGCGTTTTAGAGCTAGAAATAGC
STK39_Target_4	TAATACGACTCACTATAGGCAGGTGTCCACTCGACCCGTTTTAGAGCTAGAAATAGC
tnfa_Target_1	TAATACGACTCACTATAGGTTGAGAGTCGGGCGTTTTGTTTTAGAGCTAGAAATAGC
tnfa_Target_2	TAATACGACTCACTATAGGTCTGCTTCACGCTCCATAGTTTTAGAGCTAGAAATAGC
tnfa_Target_3	TAATACGACTCACTATAGGGATTATCATTCCCGATGAGTTTTAGAGCTAGAAATAGC
tnfa_Target_4	TAATACGACTCACTATAGGTCCTGCGTGCAGATTGAGGTTTTAGAGCTAGAAATAGC
Scaffold	AAAAGCACCGACTCGGTGCCACTTTTTCAAGTTGATAACGGACTAGCCTTATTTTAACTTGCTATTTCTAGCTCTAAAAC

690

691 **Table 3**

692 Primers used for genotyping the *oxsr1a*^{syd5} allele.

	Sequence 5‘-3‘
Oxsr1a Fw 1	aagtttggctgttgggactg
Oxsr1a Rv 1	agatgctgatgtgtggtgga
Oxsr1a Fw 2	ctgttttcagGCTCAGTGCTT
Oxsr1a Rv 2	TCCAGCCTTCACATCCctac
Oxsr1a Fw 3-4	gtttttccacagttctggtttt
Oxsr1a Rv 3-4	ccttctggaggcacaaagag

693

694 **Table 4**

695 Survival data of zebrafish embryos treated at 1 day post fertilization with varying

696 concentrations of Compound B (CB). Drug was administered once at the beginning of the

697 experiment.

	% Survival		
CB (µM)	**24hrs**	**48hrs**	**120hrs**
0.9	100	100	100
1.8	100	100	100
3.6	100	100	47
7.5	100	47	0
15	5.8	0	0
30	0	0	0

698